Printable Organic PIN Phototransistor and Its Application for Low Power and Noise Imaging Detection

Zhi Tao ⓘ, Haixin lin, Yanqing Zhu, Die Hu, Weiguang Yang, Jiangyong Pan, and Xiang Liu

Abstract—The power consumption and the opto-electric noise of organic photo-detectors are the challenges for large-scale detecting and imaging applications to surpass. This article presents a new device concept of organic heterojunction PIN channel for photo-transistor. The presence of the channel's heterostructure enables rectifying capability and effective control of defect density, which leads to low power consumption (0.12 to 7.5 nW) and low dynamic noise (4.5×10^{13} Jones detectivity). Significantly, through adopting the highly efficient Perovskite Quantum Dots as intrinsic sensing core, the device exhibits high responsivity up to 7190 A/W. As we demonstrate a large-scale 10×20 imaging array with integrated photo-transistor, the output signals are read-out and rebuilt by I-V converting amplifier with analog-to-digital circuit and numerical computation method to visualize the functionality of the system.

Index Terms—Phototransistor, perovskite, quantum dots, low noise, low power, detecting array.

I. INTRODUCTION

TO DATE, large-area organic photodetector (PD) systems are essential for many industrial applications, such as biological electronics [1] optical/touch sensors [2] and imaging applications [3]. High image quality, low-light-intensity PDs benefit greatly from a charge-amplification circuit integrated into each pixel [4]. Meanwhile, the minimum detectable signal is limited by the array's device flicker noise. However, for large-scale detecting array organic PDs are restricted by the power consumption and opto-electric noise.

Compared with photodiode PD, photo-transistor (PT) provides intrinsic amplification for photogenerated carriers enabling higher gain detection at weak light detection with higher photo-detectivity [5]. Especially, the perovskite (PVK, CsPbBr3) Quantum Dots (QDs) based PT has been reported to achieve high opto-electric performances. such as remarkable responsivity (10^4 A/W) and photosensitivity (10^3) [6]. On account of its unique characteristics, enormous efforts have been
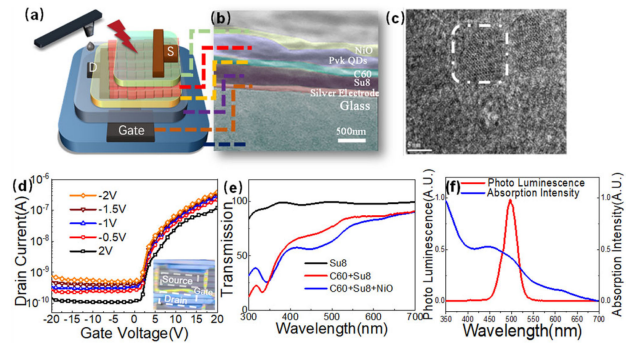
Fig. 1. (a) The structure of the C60/PVK QDs/NiO PIN photo-transistor; (b) cross-sectional SEM image for demonstrate the heterostructure; (c) TEM image of CsPbBR$_3$ QDs; (d) the electrical transfer characteristic of the PIN PT under dark with different V_{DS}; (single pixel electrodes optical image inside; the source and drain electrodes are in dotted line selected part; the gate electrode is metal luster part.); (e) the optical transmitted spectrum of the functional layers (Su8, C60, NiO); and (f) the photoluminescence spectroscopy and absorption spectroscopy of the PVK QDs.

made to construct the heterostructures in the PDs [7] for efficient opto-electric conversion, quick photo-response and low dark current. As typical n-type photoactive organic semiconductor, C60 simultaneously meet the demand of electrical and opto-electric characteristics for the detecting array [8]. Besides, due to the facile processed, Printed Electronics (PE) [9] is compatible with large-scale integrated detecting circuits. Specific intrinsic semiconductor Quantum Dots based PIN structure photo-detectors exhibit low dark current, high detectivity for the enhanced structure [10].

In this work, we present approaches to fabricate and integrate the PIN PT based on C60/Perovskite QDs/NiO and their photo-detecting circuit system with facile inkjet printing. It's technologically attractive for its low power consumption and reductive opto-electric noise. The output signals of the 10×20 sensors of the array are through noise-measuring, which are output and interpreted into a gray-scale image with the peripheral analog digital acquisition systems.

II. MATERIAL AND DEVICE PREPARATION

As shown in Fig. 1(a), the cross-sectional schematic of the printed QDs based PT demonstrates the PIN heterostructure with P-type NiO, N-type C60 and intrinsic PVK QDs' photo-sensing core.

After cleaning the glass substrate with acetone, ethanol, and deionized water successively for 10 mins, the silver gate electrode is printed on the substrate (kept at 50 °C) with a thickness of 100 nm (as illustrated in Fig. 1(b) by using 16 nozzles Q-class printhead. Then, the substrate with silver gate electrodes is baked at 110 °C for 30min allowing nanoparticles sintering. Uncross linked Su-8 2000 series photoresist (MicroChem) is dispensed at pressure of 18 Kpa and the 2 mm/s as insulating layer. After UV exposure, the Su8 layer is baked at 115 °C with 15min. After baking, the device is submitted to 2 mins UV-Ozone treatment to adjust Su8 wetting behavior ready for the printing of drain contacts. Thirdly, for printing C60 film, the 0.5 wt% concentration C60 solution is prepared with the solvent TCB(Trichlorobenzene). With the substrate keeping at 70 °C, the 100 nm C60 active layer is printed by the 16 nozzles Q-class printhead and baked at 160 °C for half an hour. After dispensing the 400 nm PVK QDs (fabricated by Dr.Pan [11]) layer with 18 Kpa and speed of 1.5 mm/s, the 200 nm NiO layer (dissolve in the Decane) is printed with the 115 °C substrates as p-type layer. Finally, after 90s UV-Ozone treatment, source electrode is printed on top of the device. The channel of the source-drain electrodes is with Width $= 80\,\mu$m, Length $= 50\,\mu$m. All devices are encapsulated with cover glasses and ultraviolet curing adhesive. Meanwhile, the devices are characterized at room temperature in a nitrogen-filled glovebox.

III. RESULTS AND DISCUSSION

As illustrated in Fig. 1(c), the high-resolution TEM image of the PVK QDs exhibits the nanoscale cubic morphology of QDs with 6.5 nm × 7.2 nm diameter. As demonstrated in Fig. 1(e), the transmission of the PIN PT is demonstrated the enhanced absorption waveband from 400 nm∼500 nm which harmonizes with the PVK QDs absorption spectrum (Fig. 1(f)).

The electrical transfer characteristic of the PIN structure photo-transistor is demonstrated in Fig. 1(d). Due to the PIN heterostructure channel, the transfer characteristic of the PIN PT exhibits 1.84 V/Dec subthreshold slope, 5.8 V threshold voltage and low driving voltage (-1.5 V). With the drain voltage ranging from -2 V to 2 V, the PIN PTs exhibits typical transfer characteristics as thin-film transistor. When the device stands dormant, the standby power is calculated as 0.12 nW from eq. 1. With the 520 nm wavelength incident light, the working power consumption increased to 7.5 nW (Fig 2(a)).

$$P = I_{DS} \times V_{DS} \tag{1}$$

In addition, transfer characteristics are investigated in Fig. 2(a) in dark under various wavelengths incident light, where photo-generated current (between drain and source) as a function of the gate voltage. The PT has 10^3 on/off ratio with the carrier mobility (9.54×10^{-1} cm^2/V·s). In corresponding with the previous absorbance properties of the PVK QDs and the other functional films, the variation of the current decreases when the incident light shifting to high visible waveband.

As illustrated in Fig. 2(b), as function of incident light power density increasing, the photo-response is more sensitive with negative drain-source voltage and the photo-current absolute
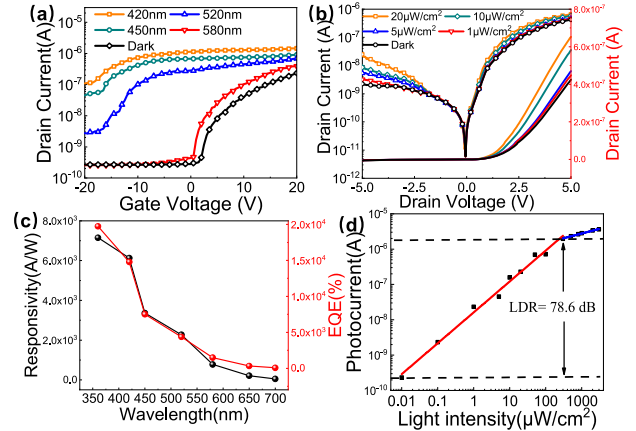

Fig. 2. (a) I_D-V_G curves for a PIN PT illuminated within the visible wavelength regime at different wavelengths (V_{DS}=5 V). (b) I_D-V_D curves for a PIN PT illuminated with various incident power density. (V_{GS}=10 V, γ=520 nm). (c) Responsivity and EQE versus wavelengths. (d) Photocurrent versus incident light power under 520 nm wavelength.

value is more obvious with positive drain-source voltage. Besides, 1 μW/cm^2 incident power density is sufficient for calculating the photo-responsivity.

The channel area can be estimated as 80 μm × 50 μm, when the incident power intensity is 1 μW/cm^2, the photo responsivity could be calculated from Eq. 2 as the opto-electric transfer characteristic curve shown in Fig. 2(a):

$$R = \frac{I_{total} - I_{dark}}{P} = \frac{I_{ph}}{\rho \cdot S} \tag{2}$$

Herein, P represents optical power, I_{total} denotes total current, I_{dark} is dark current, I_{ph} is the photocurrent, ρ indicates optical incident power density, and S is the effective area of the photoelectric reaction. By calculation of the responsivity with various wavelength, as illustrated in Fig. 2(c), with the incident wavelength deviation in the visible waveband, the responsivity decreases from the 7150 A/W to 50 A/W. Meanwhile the EQE (external quantum efficiency) decrease from the 1.9×10^4% to 71%.

$$EQE = \frac{I_{ph}/q}{\rho/h\upsilon} \times 100\% \tag{3}$$

After trying to explain the phenomenon underlying the photosensitivity of present PT under long wavelength light, it's essential to check the behavior of the responsivity as a function of the light power, which can demonstrate the application potential for the high-performance sensor along with the sensitivity characterization of the PT. Therefore, Fig. 2(d) present the variation of the photo-current as a function of the light power for 520 nm wavelength in a logarithm/logarithm plot.

Otherwise, the liner dynamic range (LDR) of the device is calculated to be 78.6 dB based on the light intensity-dependent photo-response characteristics, according to the formula [12]:

$$LDR = 20Log\left(I_{ph}/I_{dark}\right) \tag{4}$$

LDR represents light intensity operating range of the device. The relatively large LDR suggests that the recombination
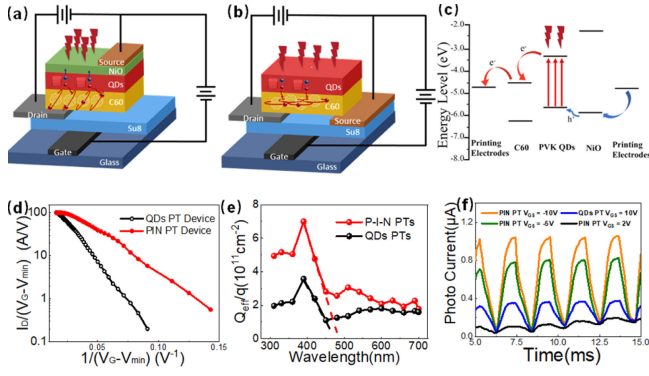
Fig. 3. (a) and (b) the schematic diagram of the photo-carriers' generation mechanism; (c) Charge transfer process within the hybrid; (d) Semi-logarithmic plot of $I_D/(V_G-V_{min})$ versus $1/(V_G-V_{min})$ for the photo-transistor with or without incident light (520 nm, 5 μW/cm^2); (e) Efficient photo-induced carriers density stored inside photo-transistor under different wavelengths; (f) Light signal response (520 nm, 5 μW/cm^2) comparison for the PIN PT and QDs PT under different gate voltage.

losses in the device are relatively low. As the major source of noise in semiconductors, the charge carrier mobility fluctuations commonly referred to flicker noise caused by the capture and release of carriers [13]. For organic semiconductors, the carriers transfer from the new band associate with the formation of donor-acceptor molecular grains [14]. Therefore, the C60 active layer is considered as a polycrystalline material and the traps sites is composed of the defect concentrated in the grain boundaries and the interface between the channel and the active layer.

For QDs based PTs (Fig. 3(b)), the excitons generated from the QDs were injected into the C60 layer by the built-in field. However, due to the influence of trap sites, the photo-generated carriers are trapped and can't be obtained effectively by the C60 layer. Based on this phenomenon, the impact of defect capture is reduced in PIN PT which is embodied in photo excitons coupled with the C60 more effectively.

A mechanism for the charge transfer within the PIN PT is proposed, where the excitons generated from QDs upon the absorption of the light energy, depending on the HOMO and LUMO levels of respective components, PVD QDs, C60, NiO (Fig. 3(c)). PVK QDs is reported to have the energy levels of HOMO and LUMO as -5.8 eV and -3.2 eV [11], respectively. The n-type C60 energy levels of HOMO and LUMO are -6.2 eV and -4.5 eV [15]. The p-type NiO energy levels are -5.9 eV and -2.2 eV [16]. Within PIN PT, heterojunction barriers not only improve the opto-electric conversion efficiency, but also should reducing the opto-electric noise. Therefore, NiO valence band effectively reduces the holes transferring within the device.

For further step, defect density could be calculated from semi-logarithmic plot for PIN PT with illumination transformation as shown in Fig. 3(d). With the link between the mobility and defect density, the conduction models in thin-film transistors with polycrystalline semiconductor layer can be applied. Both plots have a linear range. The departure from the linearity occurs at larger $1/(V_G-V_{min})$ and the slope of the linear functions is lower for with illumination than for dark current, meaning lower

slope for lower defect density [17].

$$I_D = \frac{W}{L} \mu_0 C_{ins} (V_G - V_{min}) V_D \exp$$
$$\times \left(-\frac{q^3 N_T^2 t}{8\varepsilon_0 \varepsilon_{SC} kT C_{ins} (V_G - V_{min})} \right) \quad (5)$$

W and L are the width and the length of the channel. C_{ins} is the capacitance per area unit of the gate insulator. Vmin is the gate voltage at the minimum of I_D from which the channel starts to form and then I_D start to increase. V_D is the drain voltage. q is the electronic charge. t is the thickness of the channel. N_T, is the superficial concentration of defects in the grain boundaries. S is the permittivity of the semiconducting active layer. kT is the thermal energy. From relation (5), the semi-logarithmic plot of $I_D/(V_G-V_{min})$ versus $1/(V_G-V_{min})$ may be fitted with a linear function. The slope of the function is proportional to N_T^2. As shown in Fig. 3(d), semi-logarithmic plot for QDs PT and PIN PT. Both plots have a linear range. The departure from the linearity occurs at larger $1/(V_G-V_{min})$ and the slope of the linear functions is lower for PIN PT than for PT, meaning lower slope for less defect density.

Furthermore, the effective stored charges are investigated to reveal photoexcited effective charge densities of [18]

$$\Delta Q_{eff} (\varepsilon) = C_{ox} \cdots \Delta V_{th} (\varepsilon) \quad (6)$$

With various wavelengths, the PIN PT device demonstrates a much stronger photocarrier storage capacity compared to a QDs PT. From the eq. 6, we measured the series of photo-induced threshold voltage shift ΔV_{th} and plotted ΔQ_{eff} with respect to the photo wavelength (point to the photon energy), and C_{ox} refers to geometry capacitance. Regarding any small defect density at the interface of the device since our active layer surface has few conjugate bonds in fact [8], we can expect that a considerable ΔV_{th} is only observed with the photon energy higher than the optical energy gaps of respective layer, as illustrated with their schematic band diagrams in Fig. 3(c). According to the plots of Fig. 3(e), while little ΔV_{th} is observed below 470 nm, indicating small trap density of the PIN PT.

In conclusion, based on the PIN heterostructures, the C60 layer can be coupled with the photo-carriers, which are motivated from the QDs with high efficiency. And the defect density is obviously reduced by utilized PIN structure. The dynamic photocurrent characteristics of the compared devices with different gate voltages are shown in Fig. 3(f). The photocurrent response time is affected by the photocarrier injection mechanism. Compared with QDs PT's recovery time (620 μs), the PIN PT's recovery time (320 μs) is shorter due to the padding traps among the C60 more efficiency.

To calculate the detectivity of the present devices for comparison, the detectivity D$*$ is the ability of the sensor to detect a weak signal, particularly under dynamic detecting circumstances. It characterizes the sensor relative to its noise, which can be determined from the above noise current spectrum. The detectivity is given by the following [12]:

$$NEP = \frac{I_N}{R} \left(wHz^{-\frac{1}{2}} \right) \quad (7)$$
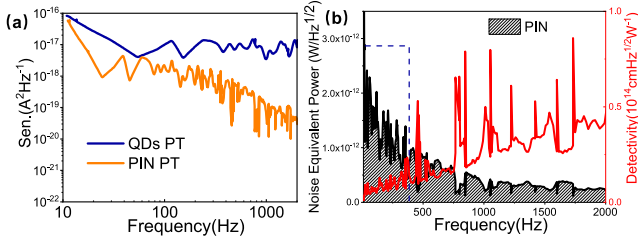
Fig. 4.   (a), (b) Noise equivalent power (NEP) and detectivity spectrum of the optimized PIN PT versus the gate frequency under a dynamic detecting environment of 386 Hz.

Fig. 5.   (a) Two-dimensional 10 × 20 array of PIN organic photo-inverter for imaging. (b) the optical micrograph showing the arrangement of pixels.

TABLE I
COMPARISON OF THIS WORK TO ORGANIC PHOTO-TRANSISTORS IN THE LITERATURE

Materials	Power (nW)	Responsivity(A/ W)	EQE (%)	Detectivity (Jones)	Reference
C60/PVK QDs/NiO	7.5	7190	1.9×10^4	4.5×10^{13}	This work
BPE-PTCDI	120	7230	3×10^3	1.9×10^{13}	[19]
ClInPc:C60	750	~	80	4.5×10^{12}	[20]
PS:C8-BTBT	4400	2200	~	10^7	[21]

$$D^* = \frac{\sqrt{A}}{NEP} \left(cmHz^{\frac{1}{2}} \Big/ w, \ Jones \right) \qquad (8)$$

Where NEP is the noise-equivalent-power, A is the active area, I_N is the noise current density and R is the responsivity. The detectivity of the PIN PT is found at the level of the lowest noise density due to the low dark current and longer diffusion length in the heterostructures (as shown in Fig. 4(a)). The PIN PT's ultimate dynamic performances can be derived and are presented in Fig. 4(b). the spectrum analyzer measurement bandwidth can be estimated by (9)

$$\int_0^\infty NEP(f) d\ (f) = NEP(f) \Delta(f) \qquad (9)$$

As obtained from the experiment phenomenon, the modulation bandwidth is 386Hz, indicating the influence of the contacted interface within the channel. The detectivity of the organic PIN PT simultaneously achieves 4.5×10^{13} Jones under a dynamic detecting environment, which is comparable to the values for the organic photo-detectors.

Compared to the reported organic photo-transistor summarized in Table I, our PIN PT has achieved outstanding responsivity, EQE, LDR and photo-detectivity. More important, this novel PIN PT can be applied in large area detecting array.

For the potential application of the large-area imaging sensor, Fig. 5(a) shows a two-dimensional 10 × 20 array of PIN PT devices (Fig. 5(b)) used for imaging light. To test the imaging sensor, optical imaging signal is projected from the 520 nm laser source whose illuminance is controlled as 5 μW/cm^2 by applying a dc voltage transformation between 0 V and 12 V.

For testing the imaging system, an opaque shadow mask with openings in the shape of the letters "NUIST" is placed in front of the detecting array. The output voltages produced by the detecting array are read and combined with the transimpedance
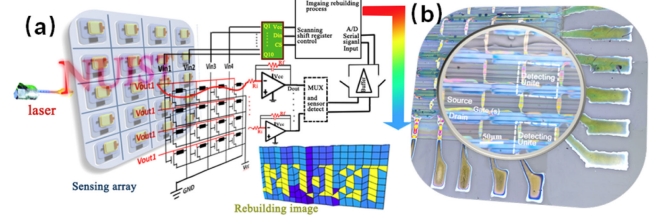
amplifier (TIA). Based on the microcurrent chip (ADA4528), the TIA circuit is utilized to realize I-V converting. And A-to-D digital signals are obtained by DAQ card. The digital signal of photo-response is rebuilt in software MATLAB as a 10 × 20 pixels images displayed on the monitor in order to visualize the functionality of the imaging system. The resolution of the rebuild image is 97%. The result can be illustrated in Fig. 5(a), which can demonstrate the resolving function of this system for different images with high distinguishing capability.

IV. CONCLUSION

In summary, we have successfully developed a low powered and low opto-electric noise photo-transistor with 7190 A/W responsivity based on a PIN hetero-structure. The EQE of the device can be improved to $1.9 \times 10^4\%$ at −1.5 V. Its peak specific detectivity at 520 nm is estimated to be about 4.5×10^{13} Jones under −1.5 V, which is comparable to commercial organic detector. Benefiting from the PIN heterostructure, the device also represented relatively large LDR (76.8 dB) with low operation power (7.5 nW). The coordination of the active layer's defect density can greatly enhance the noise immunity of the device. Meanwhile these results provide the possibility for application of the PIN PT in low-powered work mode, simple structure, low cost, and high detectivity. A complete imaging system composed of PIN PTs, the readout array, and an evaluation board, has been assembled and tested by converting the output voltages of the detecting system into an image.

REFERENCES

[1] J. A. Rogers, T. Someya, and Y. G. Huang, "Materials and mechanics for stretchable electronics," *Science*, vol. 327, no. 5973, pp. 1603–1607, Mar. 2010, doi: 10.1126/science.1182383.

[2] L. Bärgi, R. Pfeiffer, M. Mücklich, P. Metzler, M. Kiy, and C. Winnewisser, "Optical proximity and touch sensors based on monolithically integrated polymer photodiodes and polymer LEDs," *Org. Electron*, vol. 7, no. 2, pp. 114–120, Apr. 2006, doi: 10.1016/j.orgel.2005.12.002.

[3] I. Nausieda, K. Ryu, I. Kymissis, A. I. Akinwande, V. Bulovic, and C. G. Sodini, "An organic imager for flexible large area electronics," in *Proc. IEEE Int. Solid-State Circuits Conf. (ISSCC) Dig. Tech. Papers*, San Francisco, CA, USA, 2007, pp. 72–73, doi: 10.1109/ISSCC.2007.373593.

[4] K. S. Karim, A. Nathan, and J. A. Rowlands, "Amorphous silicon active pixel sensor readout circuit for digital imaging," *IEEE Trans. Electron Devices*, vol. 50, no. 1, pp. 200–208, Jan. 2003, doi: 10.1109/TED.2002.806968.

[5] Z. Tao *et al.*, "High-performance photo-modulated thin-film transistor based on quantum dots/reduced graphene oxide fragment-decorated ZnO nanowires," *Nano-Micro Lett.*, vol. 8, no. 3, pp. 247–253, 2016, doi: 10.1007/s40820-016-0083-7.

[6] H. Deng *et al.*, "Flexible and semitransparent organolead tri-iodide perovskite network photodetector arrays with high stability," *Nano Lett*, vol. 15, no. 12, pp. 7963–7969, Dec. 2015, doi: 10.1021/acs.nanolett.5b03061.

[7] Y. Fang, Q. Dong, Y. Shao, Y. Yuan, and J. Huang, "Highly narrowband perovskite single-crystal photodetectors enabled by surface-charge recombination," *Nat. Photon.*, vol. 9, pp. 678–686, Aug. 2015, doi: 10.1038/nphoton.2015.156.G.

[8] J. Mao, O. Ortiz, J. Wang, A. Malinge, A. Badia, and S. Kéna-Cohen, "Langmuir–Blodgett fabrication of large-area black phosphorus-C60 thin films and heterojunction photodetectors," *Nanoscale*, vol. 12, pp. 19814–19823, 2020, doi: 10.1039/D0NR04537C.

[9] H. Minemawari *et al.*, "Inkjet printing of single-crystal films," *Nature*, vol. 475, no. 7356, pp. 364–367, Jul. 2011, doi: 10.1038/nature10313.

[10] S. W. Shin, K.-H. Lee, J.-S. Park, and S. J. Kang, "Highly transparent, visible-light photodetector based on oxide semiconductors and quantum dots," *ACS Appl. Mater. Interfaces*, vol. 7, no. 35, pp. 19666–19671, Sep. 2015, doi: 10.1021/acsami.5b04683.

[11] J. Pan *et al.*, "Synergistic effects of charge transport engineering and passivation enabling efficient inverted perovskite quantum-dot light-emitting diodes," *J. Mater. Chem. C*, vol. 8, pp. 5572–5579, 2020, doi: 10.1039/D0TC00661K.

[12] X. Liu, L. Gu, Q. Zhang, J. Wu, Y. Long, and Z. Fan, "All-printable band-edge modulated ZnO nanowire photodetectors with ultra-high detectivity," *Nat. Commun.*, vol. 5, no. 1, Jun. 2014, Art. no. 4007, doi: 10.1038/ncomms5007.

[13] S. Martin *et al.*, "Flicker noise properties of organic thin-film transistors," *J. Appl. Phys.*, vol. 87, no. 7, pp. 3381–3385, 2000, doi: 10.1063/1.372354.

[14] K. A. Khalyfeh, A. T. Afaneh, A. Marashdeh, M. H. Almatarneh, and M. Ashram, "Thiacrown ethers engaged C60 through charge transfer: Experimental and theoretical study," *ACS Omega*, vol. 5, no. 39, pp. 25049–25058, 2020, doi: 10.1021/acsomega.0c01877.

[15] N. Wang, J. Yu, Y. Zheng, Z. Guan, and Y. J. J. o. P. C. C. Jiang, "Organic photovoltaic cells based on a medium-bandgap phosphorescent material and C60," *J. Phys. Chem. C.*, vol. 116, no. 9, pp. 5887–5891, 2012.

[16] K. Baraik *et al.*, "Epitaxial growth and band alignment properties of NiO/GaN heterojunction for light emitting diode applications," *Appl. Phys. Lett.*, vol. 110, no. 19, pp. 3112–3152, 2017.

[17] O. Bonnaud, T. Mohammed-Brahim, and D. G. Ast, *Poly-Si Thin Film and Substrate Materials*, 2004.

[18] H. S. Lee *et al.*, "MoS$_2$ nanosheet phototransistors with thickness-modulated optical energy gap," *Nano Lett.*, vol. 12, no. 7, pp. 3695–3700, 2012.

[19] X. Liu *et al.*, "Flexible organic phototransistor array with enhanced responsivity via metal-ligand charge transfer," *Acs Appl. Mater. Interfaces*, vol. 8, no. 11, pp. 7291–7299, 2016, doi: 10.1021/acsami.5b11523.

[20] C. W. Joo *et al.*, "High-performance fab-compatible processed near-infrared organic thin-film photodiode with 3.3×10^{12} jones detectivity and 80% external quantum efficiency," *Org. Electron.*, vol. 70, pp. 101–106, Jul. 2019, doi: 10.1016/j.orgel.2019.04.005.

[21] Y. Yuan and J. Huang, "Ultrahigh gain, low noise, ultraviolet photodetectors with highly aligned organic crystals," *Adv. Opt. Mater.*, vol. 4, no. 2, pp. 264–270, Feb. 2016, doi: 10.1002/adom.201500560.